Low-Energy Chlorophyll States in the CP43 Antenna Protein Complex: Simulation of Various Optical Spectra. II

ARTICLE *in* THE JOURNAL OF PHYSICAL CHEMISTRY B · AUGUST 2008

Impact Factor: 3.3 · DOI: 10.1021/jp8013749 · Source: PubMed

Low-Energy Chlorophyll States in the CP43 Antenna Protein Complex: Simulation of Various Optical Spectra. II

Mike Reppert,[†] Valter Zazubovich,[‡] Nhan C. Dang,[†] Michael Seibert,[§] and Ryszard Jankowiak*,[†]

Department of Chemistry, Kansas State University, Manhattan, Kansas 66506, , Department of Physics, Concordia University, Montreal, Quebec H4B 1R6, Canada, and National Renewable Energy Laboratory, Golden, Colorado 80401

Received: February 15, 2008; Revised Manuscript Received: April 14, 2008

The CP43 protein complex of the core antenna of higher plant photosystem II (PSII) has two quasidegenerate "red" absorption states. It has been shown in the accompanying paper I (Dang, N. C., et al. *J. Phys. Chem. B* **2008**, *112*, 9921.) that the site distribution functions (SDFs) of red-states A and B are uncorrelated and the narrow holes are burned in *subpopulations* of chlorophylls (Chls) from states A and B that are the lowest-energy pigments in their particular CP43 complexes and cannot further transfer energy downhill. In this work, we present the results of a series of Monte Carlo simulations using the 3.0-Å structure of the PSII core complex from cyanobacteria (Loll, B., et al. *Nature* **2005**, *303*, 1040.) to model absorption, emission, persistent, and transient hole burned (HB) spectra. At the current structural resolution, we found calculated site energies (obtained from INDO/S calculations) to be only suggestive because their values are different for the two monomers of CP43 in the PS II dimer. As a result, to probe the excitonic structure, a simple fitting procedure was employed to optimize Chl site energies from various starting values corresponding to different A/B pigment combinations to provide simultaneously good fits to several types of optical spectra. It is demonstrated that the shape of the calculated absorption, emission, and transient/persistent hole-burned spectra is consistent with experimental data and our model for excitation energy transfer between two quasi-degenerate lowest-E states (A and B) with uncorrelated SDFs discussed in paper I. Calculations revealed that absorption changes observed near 670 nm in the non-line-narrowed persistent HB spectra (assigned to photoconversion involving Chl−protein hydrogen-bonding by Hughes (*Biochemistry* **2006**, *45*, 12345.) are most likely the result of nonphotochemical hole-burning (NPHB) accompanied by the redistribution of oscillator strength due to modified excitonic interactions. We argue that a unique redistribution of oscillator strength during the NPHB process helps to assign Chls contributing to the low-energy states. It is demonstrated that the 4.2 K asymmetric triplet-bottleneck (transient) hole is mostly contributed to by both A and B states, with the hole profile described by a subensemble of pigments, which are the lowest-energy pigments (B_s- and A_s-type) in their complexes. The same lowest-energy Chls contribute to the observed fluorescence spectra. On the basis of our excitonic calculations, the best Chl candidates that contribute to the low-energy A and B states are Chl 44 and Chl 37, respectively.

1. Introduction

The primary processes of oxygenic photosynthetic energy transduction and charge separation occur in two functionally coupled pigment−protein complexes: photosystem I (PSI) and photosystem II (PSII) of green plants, algae, and cyanobacteria.[1] Together with a variety of peripheral antenna complexes, these two membrane-bound complexes harvest solar energy that is used to induce charge separation in "special pairs" of pigments (denoted P680 in PSII and P700 in PSI) located in the reaction center (RC) of each complex. The separated charges are then effectively channeled to separate sides of the membrane (either the plasma membrane or thylakoid membrane) to develop a proton gradient, which drives ATP synthesis. The surrounding antenna complexes assist in this process by absorbing solar energy and funneling it to the reaction center of the photosystem (PSI or PSII) with which they associate.[1] As a source of oxygen, PSII has had a profound impact on the evolution of life,[2–5] and a detailed understanding of its function is of interest both in this regard and as a model for future artificial photosystems.

Within the past decade, the crystal structure of the PSII core complex (the minimum protein preparation that can still function in oxygen evolution) has become available at increasingly detailed resolution (the best so far[6] is 3.0 Å). This structural data has revealed that the complex exists as a dimer, with each monomer containing several polypeptide chains. Two of these polypeptide chains, the D1 and D2 polypeptides, make up the RC in each monomer and bind eight pigments, six chlorophylls (Chl), and two pheophytins (Pheo).[6] Two other polypeptides, CP43 and CP47 (approximately 43 and 47 kDa, respectively) function as core antennas: they harvest excitation energy both by directly absorbing solar radiation and by accepting energy from peripheral antenna complexes associated with the system that are not part of the core.

CP43 and CP47 are structurally related,[7] and both bind just over a dozen chlorophyll pigments (13 in CP43 and 16 in CP47, according to the most recent structure of Loll et al.[6]), along

* Corresponding author E-mail address: ryszard@ksu.edu.
[†] Kansas State University.
[‡] Concordia University.
[§] National Renewable Energy Laboratory.

10.1021/jp8013749 CCC: $40.75
Published on Web 07/22/2008

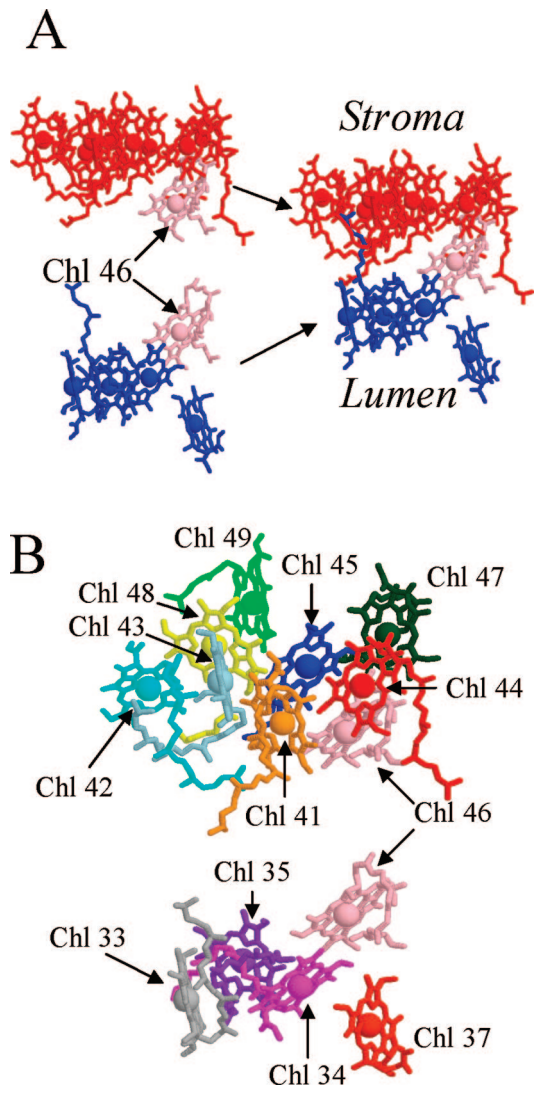

Figure 1. The Chls of the CP43 antenna protein.[6] Frame A: Chls on the stromal side of the membrane are colored red, Chl 46 (which lies in the middle of the membrane) is colored pink, and lumenal Chls are colored blue. Frame B: CP43 chlorophylls separated into stromal and lumenal groupings (Chl 46 is shown twice for clarity).

with several β-carotenes. Chls of the pigment−protein CP43 complex on the stromal and lumenal side of the membrane are shown in Figure 1A. Frame 1B labels all 13 Chls using the nomenclature of Loll et al.[6] The availability of relatively high-resolution X-ray structural data in recent years has led to several attempts by various groups to link the structure of the PSII complex (including CP43 and CP47) with experimentally determined spectral properties, providing insight into the electronic structure and excitation energy transfer (EET) dynamics within PSII.[5,8–13]

The most prominent features of a typical absorption spectrum of the isolated CP43 protein are a broad and mainly featureless absorption peak near 670 nm and a narrower and less intense peak near 683 nm, whose intensity strongly depends on the sample quality (see the accompanying paper). It appears that these two peaks represent distinct Chl pools within the complex. The higher-energy (~670 nm) pool absorbs solar radiation (or accepts excitation energy from peripheral antennas) and transfers this energy efficiently (on a time-scale of several picoseconds[8]) to the red-shifted 683-nm pigments, which act as traps at low temperature.[14,15] Then, in the intact complex, energy is transferred from the red state(s) of CP43 to the PSII RC.[16] In 2000, Jankowiak, et al.[14] demonstrated through hole-burning spectroscopy that the 683-nm peak is a sum of two quasidegenerate and weakly coupled trap states (designated states A and B). A similar conclusion had earlier been reached by Groot et al.[17] on the basis of the Gaussian decomposition of the absorption spectrum and high resolution fluorescence studies. Recent work by Hughes et al.[15] confirmed the presence of two quasidegenerate bands absorbing in this region, although in contrast to the earlier results, it was suggested that the B state may be significantly coupled to a several other chlorophylls absorbing at slightly higher energy. In addition, Hughes et al. also proposed a modified model of the hole-burning process (referred to as "photoconversion") to explain the existence of a significant buildup of photoproduct (i.e., a broadband near 670 nm) that was placed well outside the site distribution function (SDF) of the A and B states.[15] The authors suggested that the photoconversion occurs via tunneling between alternate configurations of the C═O—H−protein bond, when the molecule is in the excited state. This proposed photoconversion is discussed in this manuscript (vide infra).

The first modeling (i.e., excitonic calculations) of the absorption spectrum of the CP43 complex using the structure of the PSII core complex from *Synechococcus elengatus*[18] were reported by de Weerd et al. in 2002.[9] At that time, however, the structure used in their Monte Carlo simulations[18] was known only at 3.8 Å resolution, and the complex contained only 12 Chls (i.e., Chl 47 using the notation of Loll et al.[6] was missing). As a result, the authors of ref 9 put all the Q_y transitions in the plane of the membrane, in agreement with linear dichroism (LD) results.[17] (On the basis of the very recent CP43 structure,[6] this assumption is only in part correct; see Table 1). Using this approximation, de Weerd et al.[9] showed that the main feature of the absorption spectrum of CP43 could be roughly reproduced, with the exception of the red-most narrow absorption band near 683 nm. It was suggested, therefore, that the origin of the narrow band near 683 nm must be environmental rather than excitonic. This has been reinforced by recent analysis of time-resolved vis/mid-IR data that also suggested that the large red-shift of the origin band of some Chls could be nonexcitonic in nature.[8] On the other hand, CD results[15,17] have suggested that band B possesses significant excitonic character. Although several Chl candidates contributing to the A and B red states have been proposed in the accompanying paper, new modeling studies are necessary to provide more insight into the structure−function relationship of the CP43 complex.

To gain more insight into the electronic structure of the CP43 complex, in this study, we present results of a semiempirical calculation of Chl site energies and Chl transition dipole moments and Monte Carlo simulations of the absorption, emission, and persistent/transient HB spectra obtained for the CP43 complex with minimized contribution from aggregated CP43 complexes. In this manuscript, we do not attempt to fit the published CD spectra,[15,17] because on the basis of the absorption and HB spectra discussed in paper I, they are most likely contributed to by aggregated CP43 complexes.

It is shown that excitonic interactions assuming the same average site energy for all pigments (670 nm) and the same inhomogeneous broadening of 200 cm^{-1} (as in ref 9) do not account for the low-energy A and B states and do not fit low-temperature absorption or emission spectra or our persistent and transient HB spectra, thus confirming that, indeed, the site energies of the Chls contributing to the low-energy A and B states must be red-shifted by the protein environment they reside in[19–22] or Chl ring deformation.[23,24] A fitting algorithm was used

TABLE 1: Calculated Coupling Constants, V_{nm} (in cm^{-1}), for the Chls of CP43[a]

	Chl 33	Chl 34	Chl 35	Chl 37	Chl 41	Chl 42	Chl 43	Chl 44	Chl 45	Chl46	Chl 47	Chl 48	Chl 49
Chl 33	0	**−8.7** (−9.0)	**−3.1** (−4.8)	**−1.6** (−1.7)	**−3.3** (−3.2)	**12.4** (11.5)	**12.3** (12.3)	**1.2** (1.3)	**−7.9** (−7.7)	**2.4** (2.4)	**−1.8** (−1.7)	**−0.8** (−0.8)	**−0.1** (−0.0)
Chl 34		0	**−23.7** (−24.6)	**74.5** (81.2)	**1** (0.9)	**−6.8** (−6.3)	**−8.3** (−8.3)	**5.7** (4.7)	**22.5** (22.2)	**65.9** (64.6)	**10.8** (10.5)	**−5.7** (−5.6)	**−0.93** (−0.9)
Chl 35			0	**−19.0** (−19.6)	**−1.8** (−1.8)	**−1.2** (−1.0)	**−4.4** (−4.3)	**−5.3** (−5.0)	**−5.4** (−5.4)	**−18.6** (−17.1)	**−5.5** (−5.6)	**15.6** (15.2)	**4.7** (4.2)
Chl 37				0	**1.5** (1.5)	**3.2** (3.2)	**1.7** (1.7)	**5.7** (5.6)	**−1.2** (−1.2)	**24.0** (24.9)	**2.5** (2.7)	**−2.5** (−2.4)	**3.2** (3.3)
Chl 41					0	**−15.5** (−15.2)	**−65.6** (−64.0)	**−16.7** (−19.0)	**19.7** (21.4)	**−3.0** (−3.0)	**−1.3** (−1.4)	**2.3** (2.3)	**−3.3** (−3.5)
Chl 42						0	**51.0** (43.5)	**9.5** (9.8)	**−19.7** (−19.7)	**9.2** (9.0)	**3.7** (3.9)	**−5.4** (−5.0)	**6.9** (7.2)
Chl 43							0	**−8.8** (−8.1)	**58.9** (51.0)	**−1.2** (−0.7)	**−5.6** (−5.63)	**24.2** (20.7)	−15.7 (−15.8)
Chl 44								0	**39.7** (31.6)	**48.0** (48.5)	**47.8** (48.0)	**−16.5** (−16.0)	**8.3** (8.6)
Chl 45									0	**−36.0** (−35.8)	**86.9** (93.9)	**17.7** (12.9)	**−5.7** (−5.2)
Chl 46										0	**−58.1** (−54.8)	**−8.9** (−7.7)	**8.2** (8.0)
Chl 47											0	**−16.0** (−16.7)	**8.7** (9.6)
Chl 48												0	**−45.5** (−60.5)
Chl 49													0

[a] Bold numbers (used for simulations in this work) are calculated with the center of the Chl chosen as the average of the four ring nitrogen positions. Mg-centered constants (i.e. the position of the central Mg atom is chosen as the center of the molecule) are included in parentheses for comparison; see text for details.

to test various combinations of Chls contributing to the low energy exciton states by simultaneous fitting of several types of optical spectra. It is demonstrated that simultaneous fitting of absorption, emission, and both transient and persistent HB spectra (obtained for the CP43 complex from the same batch) allowed us to narrow the choice of Chls contributing to the low-energy A and B states. The calculated distribution of different Chls to various exciton states and their relative densities provide more insight into the electronic structure of CP43 complex. Finally, we argue that the present excitonic calculations support the model of uncorrelated EET between the quasidegenerate bands A and B, as described in the accompanying paper.

2. Material and Methods

2.1. Structural Data and Semiempirical Calculations. The crystal structure of Loll et al.[6] (Brookhaven Protein Data Bank, file 2AXT.pdb) was imported into HyperChem 7.5, which was used to add hydrogen (H) atoms to the structure (H are not resolved at the current 3.0-Å resolution). Molecular mechanics calculations using the MM+ basis set were used to optimize the positions of the H only (leaving the positions of non-H atoms unchanged). Single-point, semiempirical calculations were carried out using the ZINDO/S basis set (using configuration interaction; 25/25). In these calculations, all Chls of interest sensed the protein environment (including charged and neutral amino acids). Calculated results include the orientation of the transition dipole moments and the electronic absorption spectrum. The Q_y transition dipole moment orientation was seen to point almost directly from the ring I nitrogen (N−B) to the ring III nitrogen (N−D), so this approximation was adopted for Monte Carlo simulations (see below).

2.2. Monte Carlo Simulations. Simulations of the absorption spectrum were carried out using MathCad 12.0 and Scilab 4.1.1 (Scilab is a trademark of INRIA. See also www.scilab.org). Transition dipole moments and coupling between chromophores were calculated using the dipole−dipole approximation as in ref 12; however, due to the significant shift of the position of the central magnesium out of the chlorin plane revealed in the recent crystal structure, the transition dipole moments were taken to extend from NB to ND rather than from the central Mg to ND, and the center of the Chl molecule was taken to be at the averaged position of the four ring nitrogen atoms, rather than at the central magnesium. For completeness, coupling constants when the position of the central Mg atom was chosen as the center of the molecule are also provided (see Table 1) and tested. Both sets of the coupling constants were used to construct a Hamiltonian matrix for the CP43 chromophores; for each iteration of the Monte Carlo simulations, site energies were added randomly within a Gaussian distribution mimicking the SDF of the chromophore. Simulations were also run assuming a small distribution of the coupling constants (off-diagonal disorder) for comparison. A simple fitting algorithm was used to find optimized parameters (i.e., site energies and width of SDF) to achieve simultaneously good fits to various experimental optical spectra.

2.3. Theoretical Methods and Q_y — Excitonic Hamiltonians. Excitonic calculations for the Q_y-states were performed using the Frenkel Hamiltonian (static lattice approximation)

$$H = \sum_n (\varepsilon_n + d_n)|n\rangle\langle n| + \sum_{n,m}{}' V_{n,m}|n\rangle\langle m| \qquad (1)$$

where $|n\rangle$ denotes the localized Q_y state of Chl n, ε_n is the average Chl monomer transition energy, and d_n is the offset energy due to diagonal site excitation energy disorder that stems

from the intrinsic structural disorder of the CP43−protein complex. The vacuum dipole strength[25] for Chl *a* of 4.6 D was reduced to 4.3 D to account for the change in excitonic coupling by screening and local field effects by the dielectric environment, which corresponds to an effective dielectric constant of ∼1.42. Excitonic coupling matrix elements, V_{nm}, were calculated in the point transition dipole−dipole approximation. The neglect of the electron-exchange coupling contribution to V_{nm} is reasonable given that the center-to-center distances among the vast majority of Chls are at least about 9 Å. The model Hamiltonian for the Q_y states is defined by the numbers in Table 1.

In our first approach (vide infra), ε_n values were set equal to 14 925 cm^{-1} (∼670 nm) for all Chls, as in ref 9. However, it was found that this assumption provided very poor fits to the experimental spectra, and a simple fitting algorithm was introduced to generate site energies that fit various types of spectra (see Section 2.2). Diagonal energy disorder was taken into account by Monte Carlo simulations with random disorder at each Chl described by a Gaussian SDF, as discussed above. Guided by low-temperature absorption spectra, the original value of the site (excitation energy) distribution function for each cofactor was assigned a width of 180−250 cm^{-1}; the SDFs of the Chls were taken to be uncorrelated. For each realization of Chl site energies, the Hamiltonian matrix was diagonalized to obtain the excitonic energies (E_α) and wave functions

$$|\alpha\rangle = \sum_n c_{\alpha n}|n\rangle \tag{2}$$

Since overlap is neglected, $\sum_n |c_n^{(\alpha)}|^2 = 1$ The excitonic transition dipoles were calculated using:

$$\vec{\mu}_\alpha = \sum_n c_n^{(\alpha)} \vec{\mu}_n \tag{3}$$

where $\vec{\mu}$ is the transition dipole of Chl *n*. The optical properties of each CP43 complex were calculated using the eigenvalues and eigenvectors. Absorbance spectra and the contributing bands from the 13 exciton states were obtained by an ensemble-averaging with energetically sorted eigenvalues and corresponding eigenvectors. Absorbance and delta absorbance spectra were calculated with 5 cm^{-1} resolution. All results presented correspond to ensemble averaging over 20 000−50 000 CP43s. The spatial extent (delocalization) of the exciton states (N_{del}) was calculated using $N_{del} = 1/\sum_n |c_n^{(\alpha)}|^4$ where N_{del} is the number of Chls that contribute to the exciton state, α. The density of exciton states is given by

$$d_\alpha(\omega) = \left\langle \sum_\alpha \delta(\omega - \omega_\alpha) \right\rangle_{dis} \tag{4}$$

and is compared in Figures 5 and 7 with the exciton states Chl distribution given by eq 5,

$$d_n(\omega) = \left\langle \sum_\alpha \left|c_n^{(\alpha)}\right|^2 \delta(\omega - \omega_\alpha) \right\rangle_{dis} \tag{5}$$

where $\hbar\omega_\alpha$ is the energy of the α^{th} exciton state and $|c_n^{(\alpha)}|^2$ is the probability that Chl *n* is excited in the αth exciton state.

2.4. Simulation of Transient and Persistent HB Spectra. Simulated transient and persistent HB spectra were generated simultaneously with absorption spectrum calculations. For each iteration of the absorption spectrum calculation, the calculated eigenvalues and eigenstates were sorted by energy. The "lowest state" Chl was identified by selecting the maximum absolute value, $c_{\alpha n}$, coefficient for the eigenvector corresponding to the lowest energy eigenstate (i.e., the Chl corresponding to the maximum eigenvector entry). The site energy of the "burned" lowest state Chl was then placed randomly within a Gaussian distribution that simulates the new site energy of burned pigments (persistent hole) or the triplet state absorption frequency (transient hole). The site energies of all other chloro-

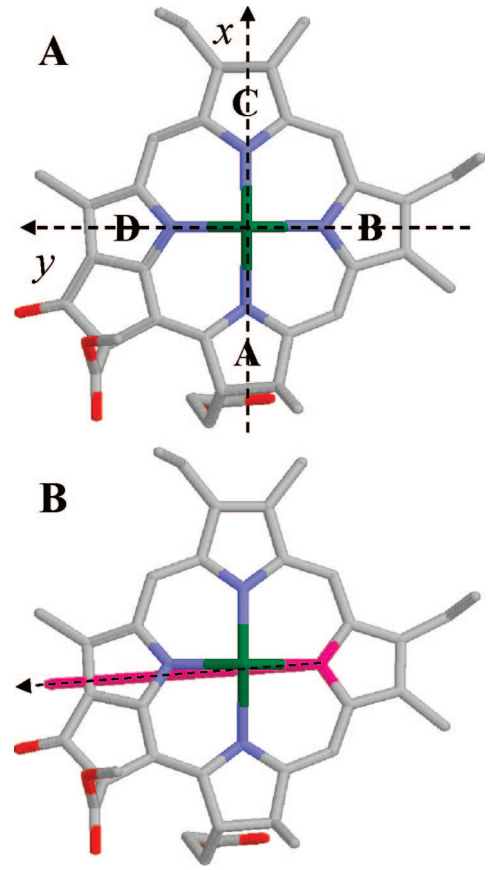

Figure 2. Frame A: Chl 42 (Cla42 in the nomenclature of Loll et al.[6]) with labeled rings and molecular *x* and *y* axes. Frame B: calculated transition dipole moment of Chl 42. The calculated transition dipole departs by 4.6° from the axis extending from nitrogen B to nitrogen D (the largest deviation of any of any transition dipole moments calculated in this work from the NB-to-ND approximation).

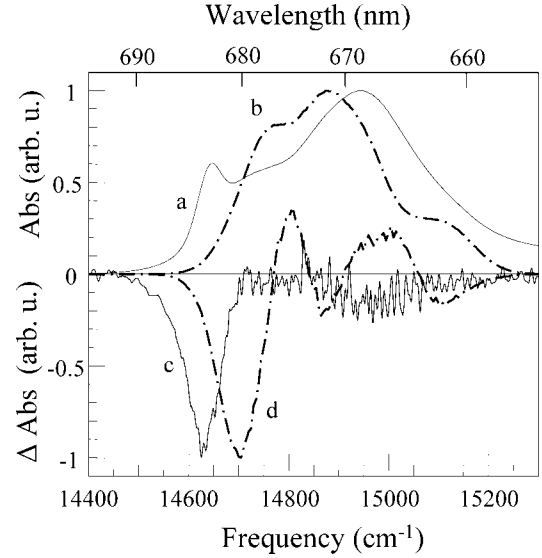

Figure 3. Experimental (solid) and calculated (dot−dashed) absorption (curves a and b) and triplet bottleneck hole (curves c and d) spectra for the CP43 complex using the site energies and distribution widths of De Weerd et al.:[9] all Chl site energies are set to 14 925.4 cm^{-1} (670 nm), and all distributions have a fwhm of 200 cm^{-1}.

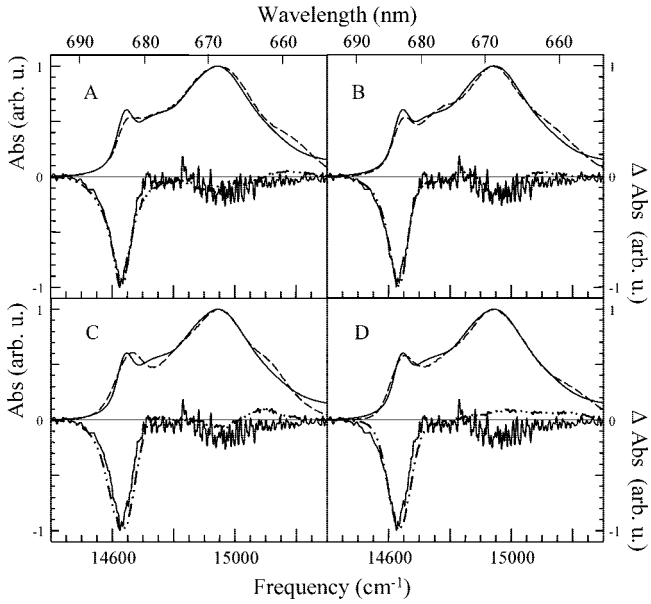

Figure 4. Experimental absorption (smooth, solid curves) and triplet bottleneck hole (noisy, solid curves) spectra of CP43 are shown in all frames together with calculated absorption (long-dashed curves) and transient (dash−dot−dotted curves) spectra of CP43 obtained for various pigment site−energy combinations. The site energies for the calculated curves were obtained using a fitting procedure for the following A/B pairs (see text for details): A41/B44 (frame A), A37/B44 (frame B), A44/B37 (frame C), and A43/B37 (frame D).

phylls remained unchanged from those used to calculate the iteration's original eigenvalues. The transient or persistent HB spectrum was then calculated using the new set of site energies. For the transient hole simulation, the lowest-energy chlorophyll was placed near ∼865 nm to mimic the corresponding triplet state energy,[26] thus effectively decoupling it from the rest of the pigments in the complex. To simulate the persistent hole-burned spectrum, the site energy of the burned lowest energy pigment was randomly chosen from a Gaussian SDF, generally shifted from the respective pigment's "pre-burn" SDF, either to the red (B-state antihole) or to the blue (A-state antihole). These SDF shifts were used as experimentally constrained parameters in attempts to fit the persistent hole burned spectrum.

2.5. Fitting Procedure. For a given choice of Chls A and B, site energies were chosen for all Chls of the complex using a simple algorithm to simultaneously fit the experimental absorption and transient hole spectra of CP43. In this algorithm, the quality of the fit to each spectrum is assessed by the root-sum-square of the difference between the corresponding calculated and experimental spectra (i.e., the norm of the difference vector formed by subtracting the *y*-values of the experimental spectrum from the *y*-values of the calculated spectrum). For simultaneously fitting absorption and transient holes, the root-sum-square values for both spectra are added. For a given choice of A/B pigments, the initial site energies of the two Chls chosen as candidates for A and B are both set to 681 nm (∼14684 cm^{-1}), whereas the site energies of the remaining pigments are set identically to 668 nm (∼14970 cm^{-1}). The standard deviations of distribution functions for the pigments chosen as A and B are set to 90 and 30 cm^{-1} (fwhm ∼ 212 and ∼71 cm^{-1}), respectively; the remaining pigments are given distribution functions with standard deviations of 100 cm^{-1} (fwhm ∼ 236 cm^{-1}). Using these starting parameters, initial absorption and transient HB spectra (and the corresponding root-sum-square values) are calculated (5000 iterations of the Monte Carlo simulation at a resolution of 20 cm^{-1}). The site energy distribution center values of all pigments and the distribution function widths of the A- and B-state pigments are then varied one by one (the distribution widths of the non-A/B pigments remains fixed). After each variation, the calculation is repeated (5000 iterations at 20 cm^{-1} resolution) if the root-sum-square value of the second set of calculated spectra is lower than the previous root-sum-square value, the initial set of parameters (and root-sum-square value) is replaced with the altered set; otherwise, the new set is rejected. Since the algorithm is intended to fit the spectra for a chosen A/B pair, the A/B site energies are required to change rather slowly to prevent either Chl of the A/B pair from shifting too much to the blue. As a result, at each variation of average site-energy values, a new A- or B-pigment site energy center value is chosen randomly within a Gaussian distribution about the previous site energy center value (standard deviation = 10 cm^{-1}). Similarly, to prevent the A and B pigments from "switching" with each other, their distribution widths are prevented from changing too abruptly in a given variation by choosing standard deviations for the A and B state SDFs randomly within a normal distribution about the previous value (standard deviation = 2 cm^{-1}). Since no restrictions are imposed on the site energy center values of non-A/B pigments, at each variation, a new site energy center value is chosen randomly within the range 14 641 cm^{-1} (683 nm) to 15 151 cm^{-1} (660 nm). That is, the new center value is uncorrelated with the previous value and is given by 14 641 cm^{-1} plus a random number between 0 cm^{-1} and 510 cm^{-1}.

For each choice of A/B pigments presented below (see Figure 4), 1500 variations were tested: 100 variations for each of the 13 site energy center values and each of the two distribution widths for the A and B state pigments. This 1500-variation procedure was then repeated 10 times (a total of 15 000 variations tested) for each A/B pair, and the best set of site energies was then selected from the resultant 10 best-fit spectra (for each A/B pair). A modified final optimization procedure, in which each spectrum was calculated at 10 cm^{-1} resolution (using 10 000 iterations of the Monte Carlo simulation) was applied to each set of site energies. In this procedure, all pigments were treated equivalently like the A and B state pigments in the above fitting procedure to prevent rapid changes (i.e., at each variation, site energy center values and distribution widths were chosen from a normal distribution around their current value). The distribution widths for non-A/B pigments varied only negligibly during this final optimization, and for simplicity of presentation, the curves presented in Figure 4 have non-A/B pigment distribution widths fixed at σ = 100 cm^{-1}.

2.6. Experimental Absorption, Emission, and Persistent/Transient HB Spectra. Transient and persistent HB spectra were taken from the accompanying paper. The details of the low-temperature HB setup used are described in refs 27–29. Briefly, the absorption and HB spectra (at 4 cm^{-1} resolution) were recorded with a Bruker HR125 Fourier transform spectrometer. Nonresonant burning was performed with green light optimized at 496.5 nm from a Coherent Innova 200 Ar^+ ion laser. Fluorescence was dispersed by a 300-mm-focal-length spectrograph (PI Acton) and detected by a PI Acton Spec-10 (1340 × 400) CCD camera (for details, see paper I). Spectral resolution for fluorescence spectra was 0.1 nm. The persistent nonphotochemical hole-burned (NPHB) spectra reported correspond to the postburn absorption spectrum minus the preburn absorption spectrum. The triplet bottleneck (transient) hole spectra correspond to absorption spectrum with laser *on* minus the spectrum with laser *off*. Transient hole spectra were

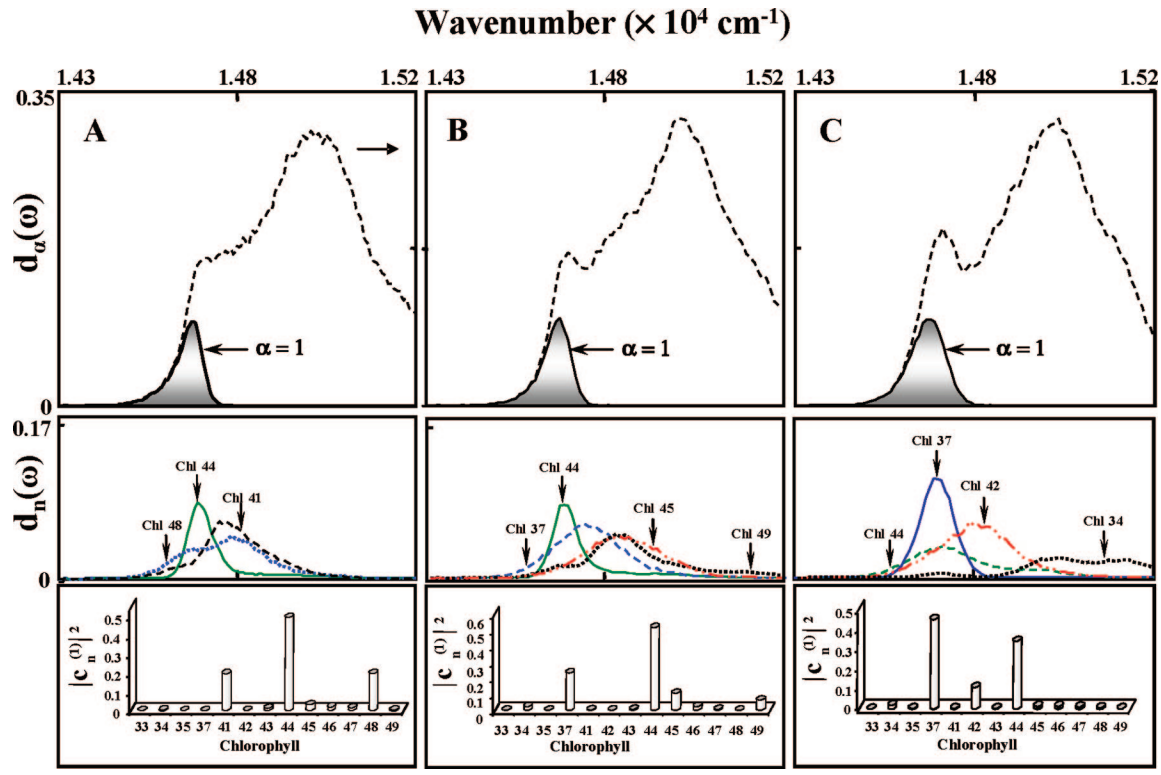

Figure 5. Frames A (for A41/B44), B (for A37/B44), and C (for A44/B37) in the top and middle panels show the density of the lowest-energy exciton state ($d_{\alpha=1}(\omega)$; the shaded bands) and the corresponding Chl distribution $d_n(\omega)$, respectively. Calculated absorption spectra (equivalent to those reported in Figure 4, frames A, B, and C) are shown as long-dashed line spectra in the top panels. The corresponding averaged occupation number of the Chls contributing to the lowest-energy exciton state is shown in the lower panels (see text).

measured after the persistent hole-burning process had reached saturation (for more details, see paper I).

3. Results

3.1. Site Energies, Transition Dipole Moment Orientations, and Coupling Constants. ***(a) Site Energies of Various Chls.*** The site energies of Chls in photosynthetic complexes may significantly vary from pigment to pigment and from those in solution, complicating spectral simulations. That individual Chls in protein environments have different site energies is not surprising because polarity in the local environment, formation of hydrogen bonds with the surrounding protein[8]), and different ring deformation[24] of a particular Chl may lead red shifts of their absorption origin bands. In addition, as suggested by Balaban et al.,[21,22] concerning PSI Chls, β-ligated pigments may also experience a red shift of the transition energy compared to α-ligated ones. Unfortunately, site energies of individual pigments in excitonically coupled systems cannot be easily obtained experimentally. Theoretical predictions of site energies, whether calculated quantum mechanically (QM)[13] or extracted by a genetic algorithm described in ref 11 may also significantly vary as illustrated by the markedly different parameters obtained for the PSII RC by various groups. For example, Vasil'ev et al.[13] and Raszewski et al.[11] obtained site energies for the P680 Chls ($P680_1/P680_2$) of 672/672 and 666/666 nm, respectively, while the site energies of pheophytins $Pheo_1/Pheo_2$ were placed at 666/681[13] or 672/675 nm.[11]

It has recently been demonstrated by Zucchelli et al.[24] that site energy variations in the peridinin−chlorophyll−protein (PCP) complex and light-harvesting complex II (LHCII) can be partially accounted for by considering the effects of macrocycle deformation on Chl energy levels. Briefly, Chl out-of-plane distortions are described in terms of an orthonormal basis set (with corresponding deformation energies) developed by Jentzen and co-workers.[30] Adjustments to Chl molecular orbital energies are then evaluated on the basis of their symmetry and the symmetry of the various normal mode deformations, and the Q_y transition energy is estimated, allowing for partial mixing between HOMO → LUMO and HOMO − 1 → LUMO + 1 transitions.[24] Significantly, using this method, Zucchelli et al. were able to largely account for the significant red shift of CLA612 in the 2.72-Å resolution crystal structure of LHCII[31] (Brookhaven Protein Databank ID 1RWT).[24] Unfortunately, the 3.0-Å resolution of the current PSII structure is most likely not sufficient for this method to accurately be applied to the CP43 protein. Preliminary calculations performed after the method of Zucchelli et al.[24] (not included in this publication for brevity) identified Chl 37 as being the most significantly red-shifted Chl in the CP43 complex, but no Chl exhibited a shift of more than a few nanometers (in contrast to the 17-nm redshift of CLA612 in Zucchelli's analysis of LHCII); a more detailed analysis will have to await a higher resolution crystal structure. In addition, since Chl ring deformation is only one of many factors contributing to site energy variations among Chl molecules in pigment−protein complexes, this method, while very useful, cannot alone unambiguously assign transition energies.

Because of these difficulties, site energies are the most uncertain parameters in simulations of various optical spectra of CP43 and other pigment−protein complexes. Of course, in principle, the best approach to get proper site energies would be to use quantum chemical (QChem) calculations. Unfortunately, the size of this protein complex and the current resolution (3.0 Å) make this task very difficult, if not impossible. Regarding the site energies of Chl *a* in the CP43 complex, Vasil'ev and Bruce,[13] on the basis of QM calculations and molecular dynamics simulation on the lower resolution (3.50 Å) structure

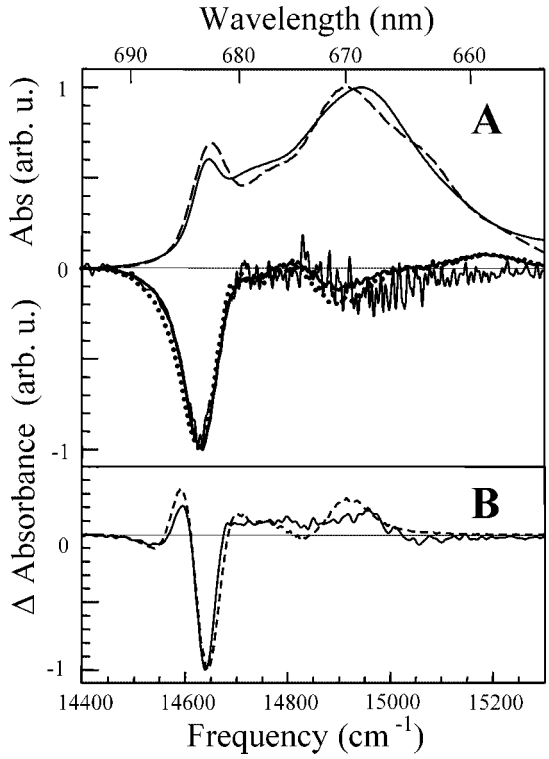

Figure 6. Experimental CP43 spectra and calculated spectra using best-fit parameters for the A44/B37 pair (see Table 2). Frame A: experimental (smooth, solid curve) and calculated (long-dashed curve) absorption spectra of CP43 together with experimental (noisy, solid hole) and calculated (solid and dotted holes) triplet bottleneck hole spectra of CP43. The dotted transient hole-burned curve corresponds to the calculated transient hole-burned spectrum when Chl 44 (pigment A) contributes to the spectrum with twice the efficiency of all other Chls; note the increased hole depth in the 670-nm region. Frame B: experimental (solid curve) and calculated (dashed curve) persistent hole-burning spectra of CP43. Site energies and distribution widths for the A and B states were obtained via a fitting algorithm and manual adjustment of final parameters to obtain fits for all three spectra (see text for details).

of PSII,[32] showed that the Q_y transition energies of Chls in CP43 span the spectral range of about 20 nm, with the average site energy at ~674 nm. Unfortunately, the site energies for Chls of the CP43 complex reported by Vasil'ev and Bruce,[13] using a static disorder of about 180−250 cm^{-1} and our coupling constants calculated from recent X-ray structure[6] (see Table 1) do not fit the CP43 low-temperature absorption, fluorescence, or HB spectra (data not shown).

To obtain site energies for pigments in the CP43 complex, we performed ZINDO/S calculations on both sides of the PSII dimer, using the more recent 3.0-Å resolution structure of Loll et al.[6] Interestingly, calculations on opposite sides of the PSII dimer resulted in different site energies for the Chls. Since the two sides of the PSII dimer should be rather identical, this is most likely a result of the insufficient current resolution of the crystal structure. Although it may well be that the level of quantum mechanical calculations performed here is not rigorous enough to accurately reproduce the electronic spectra of such a large system, energy shifts on either side of the dimer would be expected to at least bear some correlation to each other. The fact that they do not seems to suggest that, at the current resolution, not even more advanced calculations will be able to accurately predict Chl site energies. Despite the obvious discrepancies, site energies from both sides of the dimer have some common trends. The most obvious is that, on both sides of the complex, Chls 44 and 47 are very much red-shifted. Chl 42 is significantly red-shifted on side one of the dimer but much less so on side two, whereas Chls 37 and 41 are moderately red-shifted on both sides. This suggests that some of the above-mentioned Chls should contribute to the lowest-energy states observed experimentally (see paper I), although given the discrepancies between the two sides of the PSII dimer, the calculated site energies are tentative and should still be treated as adjustable parameters, as done in this work (vide infra).

In light of the above discussion, we believe that structure-based calculations alone are not sufficient to predict site energies in the absence of interpigment interactions with high accuracy, although they may provide some insight on the possible red shifts. Thus, additional spectroscopic information on individual Chls contributing to various spectral bands (e.g., Chls contributing to the low-energy traps) is needed to decrease the number of variables in modeling of optical spectra. In the case of CP43, fortunately, the differences observed between different types of experimental hole-burned (HB) spectra (see paper I) which result from different physical processes provide information on the Chls contributing to the lowest energy A and B states. Together with indications of moderate coupling strength between these two states,[33] their relative dipole moment orientations, and their relative location with respect to the RC,[6,15,34] such experimental data can narrow the choice of possible Chls contributing to the low-energy excitonic states, providing parameters which can be further tested and refined in modeling studies.

Therefore, Monte Carlo simulations have been performed with various combinations of site energies, keeping in mind the following: (1) the lowest absorption band near 683 nm has to be contributed to by at least two Chls/states with significantly different SDF widths, to be consistent with the HB data[14,15,33,35,36] (various combinations of Chls assigned for the A and B states need to be tested); (2) pigments contributing to states A and B should be relatively weakly coupled (V_{nm} ~ 5−12 cm^{-1}), as predicted by data reported in ref 33 to ensure EET on an ~10-ps time scale; (3) at least one of the pigments contributing to the low-energy states preferably should be located close to the RC[15,34] (e.g., Chls 41, 44, 37, and 34); (4) the oscillator strength of the lowest exciton band (obtained as a result of energy sorting), which predominantly contains contributions from both A and B bands, must be lower than 1 to fit measured transient hole-burned spectra (see paper I); and (5) the combined oscillator strength of the two lowest exciton states should be smaller than 2 in order to fit the negative absorbance decrease near 669 nm (vide infra). In addition, fits to the unique shape of the nonresonant persistent hole burned spectrum (in particular, the broad positive ΔA with maximum near 670 nm) could further limit the possible choices of Chls contributing to the lowest energy states.

(b) Q_y Transition Dipole Moments. For coupling calculations, the dipole moment of Chl *a* is frequently approximated as extending from NB to ND (see, for example, see refs 34 and 37. To check this assumption, the dipole moments obtained via ZINDO/S calculation, based on the recent structural data of CP43,[6] were compared with those obtained using the NB-to-ND approximation (see Figure 2). It was found that the calculated dipole moment vectors were in general in very good agreement with the above-mentioned approximation, although variations for the 13 Chls of CP43 complex (on the order of 1.5−4.6°, depending on Chl) were observed. The calculated transition dipole moment of Chl 42 of CP43 (which showed the largest deviation of 4.6° of any Chl from the NB-to-ND

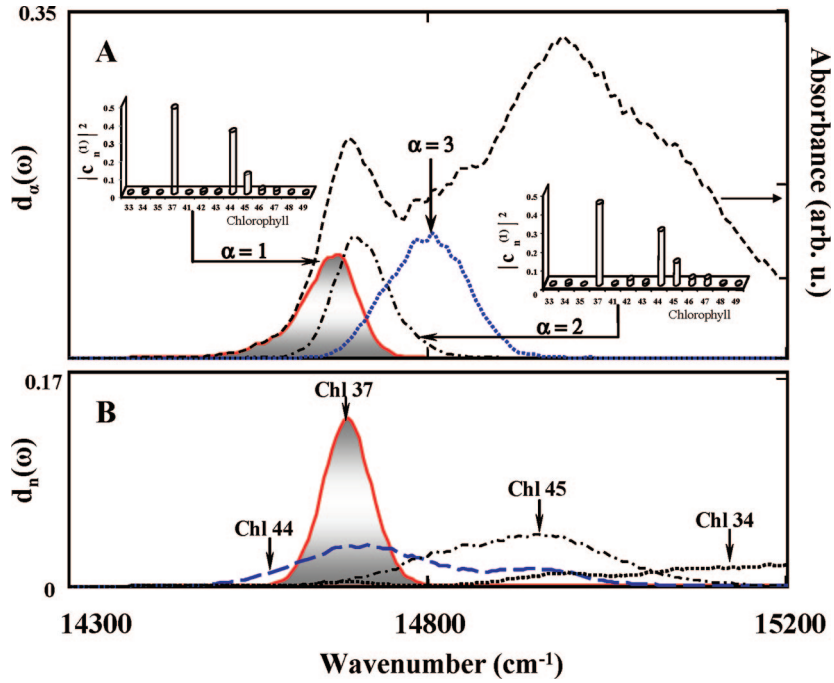

Figure 7. Frame A: The dashed line is the calculated absorption spectrum for the best combination of Chls contributing to the A and B states (i.e., A44/B37); see Table 2 for parameters. The density of the three lowest-energy exciton states is shown below as the solid, dash-dotted, and dotted lines, respectively. The left and right inserts show the averaged occupation number of the major Chls contributing to the first and second exciton states ($\alpha = 1$ and $\alpha = 2$, respectively). Frame B: Distribution functions, $d_n(\omega)$, of Chl 37, 44, 45, and 34 plotted as a function of energy (see text for details).

TABLE 2: Chl Site Energies (E) and Corresponding Wavelengths (λ) in CP43 Complexes Obtained by Optimization of Four Types of Optical Spectra Shown in Figures 6 and 8

Chl #	Ch33	Chl 34	Chl 35	Chl 37	Chl 41	Chl 42	Chl 43	Chl 44	Chl 45	Chl 46	Chl 47	Chl 48	Chl 49
λ (nm)	668.5	660.4	660.9	682.0	664.3	671.8	664.6	680.3	674.6	668.5	668.9	668.9	667.8
E (cm^{-1})	14959	15142	15131	14663	15053	14885	15047	14700	14824	14959	14950	14950	14975
fwhm	235	235	235	73	235	235	235	188	235	235	235	235	235
ligation	α	α	α	β^a	α	α	β^b	α	β	β	α	β	α

[a] The ligation status of Chl 37 is difficult to assign (see Figure 9 and text for details. [b] The only noncarbon atom resolved within 5.0 Å of Chl 43 is the hydroxyl oxygen atom of Ser 275. The oxygen appears to be in a favorable orientation for ligating the Mg atom. Interestingly, this residue was not listed among the conserved residues reported in the sequence comparison study of Bricker and Frankel[7]. The real ligand could well be an unresolved water molecule.

approximation) is shown in Figure 2B, as an example. However, these small variations had little effect on the calculated V_{nm} values. Given the relatively small effect such differences caused in calculated optical (linear) spectra (data not shown for brevity), it was assumed that the NB-to-ND approximation was sufficient for the calculations that follow.

(c) Coupling Matrix Elements, V_{nm}. Calculated coupling constants for the Chls of CP43 are listed in Table 1. Bold numbers are calculated with the center of the Chl chosen as the average of the four ring nitrogen positions. Mg-centered constants (i.e., the position of the central Mg atom is chosen as the center of the molecule) are included in parentheses for comparison. Although both sets of V_{nm} values were used in preliminary calculations, the small differences in the V_{nm} values obtained by these two different approaches had only a slight effect on the calculated optical spectra; unless otherwise noted, all calculations reported here use the coupling constants shown in bold in Table 1.

3.2. Calculated Absorption and Transient HB Spectra and the Nature of the Lowest-Energy Exciton States. ***(a) Simulated Absorption and Transient HB Spectra Obtained with Identical SDF and Site Energies.*** As described in the Introduction, De Weerd et al.[9] have previously performed Monte Carlo simulations of the CP43 absorption spectrum. However, because the 3.8-Å resolution structure[18] used by De Weerd et al. resolved only the Chl rings and could not assign NB and ND nitrogens, they assumed that all transition dipole moments lay within the membrane plane. Since new structural data has become available, we begin our modeling studies with the simulated absorption spectrum using the distribution parameters of De Weerd et al.,[9] but with coupling constants and dipole moments calculated from the more recent crystal structure of Loll et al. using the NB-to-ND approximation. That is, the Q_y-transition energies of Chls were set to 670 nm, assuming a static disorder of 200 cm^{-1} (i.e., inhomogeneous full width at half-maximum (fwhm)). For direct comparison, coupling constants were calculated using the Mg atom as the center of the interacting pigments and an oscillator strength of 24 D^2 as in ref 9. This recalculation is warranted, since the more recent structure of Loll et al.[6] resolves 13 CP43 Chls (the older structure of Zouni et al.[18] resolved only 12) and since the new structure reveals several pigments that have transition dipole moments forming an angle of ~20° or more with respect to the membrane plane. The calculated absorption and transient hole-burned spectra (dot−dashed curves b and d, respectively) are presented in Figure 3, along with the corresponding experimental spectra (solid curves a and c). Due to the differences in resolution and Chl coordinates between the two crystal structures, it is not

surprising that the shape of our calculated absorption spectrum differs significantly from the spectrum obtained by de Weerd et al.[9] (not shown). The calculated absorption spectrum in Figure 3 (curve b) is much narrower than the experimental absorption spectrum (curve a), and the gap between the low-energy shoulder and the main maximum is much too small compared with the measured spectrum. As a result, the calculated transient hole (curve d) is broader and significantly blue-shifted in comparison with the measured transient hole (curve c). In addition, the calculated transient hole-burned spectrum (in disagreement with experiment) shows strong positive bands near 665−670 nm. The lowest energy exciton state (data not shown) is mostly contributed to by Chl 45 (with an occupation number of 0.19), followed by 47, 43, 45, and 34. It is, needless to say, that the absorption and transient HB spectra (and the composition of excitonic states) calculated in this way cannot explain the zero-phonon action spectrum or the HB or fluorescence spectra discussed in paper I.

(b) General Approach to Simulation of Various Optical Spectra. In light of the data shown in Figure 3, it is clear that at least two or three pigments must be shifted significantly red to fit the experimental CP43 spectra. In addition, to account for the narrow absorption band at 683 nm, at least one of these pigments has to have a narrow inhomogeneous width (fwhm on the order of 40−70 cm^{-1}). These requirements are strongly supported by the HB data presented in paper I. In light of the above remarks, our simulations are based on a fitting procedure in which different pairs of pigments are shifted to the red and the site energies of these two pigments and the remaining pigments in the complex are optimized by a simple fitting algorithm (vide supra). In each fit, one of the two red-shifted pigments (selected as state B) is assigned a narrow inhomogeneous broadening, while the other red-shifted pigment (state A) is assigned a larger inhomogeneous broadening in agreement with experimental HB data. We emphasize that shifting just one pigment, responsible for the band B, was not enough to account for the low-energy edge of the experimental absorption spectrum and the experimental HB data.

(c) Experimental Constraints on the Low-Energy Pigment Composition. Preliminary fitting of CP43 spectra showed that the absorption spectrum alone can be well-fitted with several sets of site energies and different pairs of Chls assigned to the states A and B, although the great majority of these parameter sets did not fit other experimental spectra (i.e., transient and persistent HB spectra). However, as discussed in the Introduction, we will invoke a number of experimental constraints to limit the number possible A/B combinations and site energies for all pigments. First, the shape of the transient HB spectra (in particular the hole near 669 nm) discussed in paper I clearly suggests that the oscillator strength of the first state and of the two lowest-energy exciton states, must be smaller than that of one and two Chl molecules, respectively (see paper I). In addition, on the basis of our recent work on the PSI-CP43′ supercomplex in which states A and B were also observed experimentally and assigned to CP43′, the coupling between Chls contributing to states A and B should be relatively weak, that is, 5−12 cm^{-1}. Originally, it was suggested in ref 14 that interaction between the two pigments is extremely weak, but more recent HB work on CP43 (see paper I) and the PSI-CP43′ supercomplex[33,36] suggests that coupling should be of sufficient strength to allow for excitation energy transfer on a time scale of about 10 ps. The latter, and the requirement that at least one of the lowest-energy pigments should be close enough to the RC to allow for efficient EET to the RC, further limits the choice of low-energy pigments, as discussed in the next subsection.

(d) Possible Chls Contributing to States A and B. The most strongly coupled Chls of the CP43 complex to the RC pigments, which could participate in fast EET, are Chls 41, 44, 37, and 46. As a starting point for our calculations, it was assumed that at least one of these four pigments should contribute to one of the low-energy states (either A or B). Absorption simulations were then carried out for all possible A/B pairs consisting of one of these Chls with another Chl for which the coupling was smaller than 25 cm^{-1}. On the basis of oscillator strengths of the 683 nm absorption band in these calculations (see above subsection), this screening revealed that the most likely candidates for the red-shifted Chls are Chl 37, 41, 44, and 49, although Chl 34 cannot be excluded. Regarding Chl 49, it is unlikely that this pigment contributes strongly to the lowest exciton state, since no spectral changes were observed in emission of the PSII core complex upon mutation of His119 (the ligand of Chl 49) to either glutamine or tyrosine,[38] suggesting that Chl49 does not contribute strongly to the A or B states, as emission from substates A_s and B_s (see paper I) contributes to CP43 fluorescence. This leaves only four pigments that are likely to contribute to A/B or B/A pairs (12 different distinguishable combinations). On the basis of the very strong coupling between Chls 34 and 37 (75 cm^{-1}), this pair can be excluded, leaving 10 possible combinations to be further tested.

From the point of view of CP43 Stark experiments,[14] the most likely candidate for state B should be Chl 37 or Chl 34, since the transition dipole moments of these two strongly coupled pigments ($V_{nm} = 75$ cm^{-1}) are nearly perfectly antiparallel. Note that Chl 37 was also found to be red-shifted on the basis of ring-deformation calculations (vide supra), although given the poor resolution of the structure, these calculations should be considered preliminary. If Chl 37 is indeed strongly contributing to the state B, the most likely candidate for state A is Chl 44 (and not Chl 41), since Chl 41 and Chl 37 are too weakly coupled to account for experimental data reported in ref 33. Nevertheless, all 10 pigment combinations involving Chls 34, 37, 41, and 44 were tested, along with several other weak candidates, to see whether the above reasoning is supported by more rigorous excitonic calculations as, described in Sections 3.3−3.5.

3.3. Optimized Absorption and Transient Spectra for Various Combinations of Chls Contributing to Lowest Energy States. Experimental absorption (smooth, solid curves) and triplet bottleneck hole (noisy, solid curves) spectra of CP43 are shown in all frames A−D of Figure 4, together with calculated absorption (long-dashed curve) and transient (dash−dotted curve) spectra of CP43 obtained for various pigment site−energy combinations. The site energies for the calculated curves were obtained using the fitting procedure described in the Methods section for the following A/B pairs: A41/B44 (frame A), A37/B44 (frame B), A44/B37 (frame C), and A43/B37 (frame D). These four combinations were chosen as representative of all the combinations tested (including all 10 of the A/B pairs discussed in the preceding section). As shown in Figure 4, all these combinations provided good fits to the absorption spectrum, although in contrast to the data shown in frames A−C, the transient spectrum in frame D (corresponding to the A43/B37 Chl pair) shows an obvious discrepancy with the experimental curve (noisy, solid line) in the region near 669 nm. In addition to these combinations, the A34/B44 combination provided a reasonable fit to both absorption and transition hole spectra; however, the spectrum is very similar to that shown in

frame B for the A37/B44 combination and is not shown for brevity. It is worth noting that although many combinations provided good fits to the experimental absorption spectrum, only those combinations in which Chl 44 was either A or B provided reasonable fits to the transient hole spectrum (i.e., showed a bleach near 670 nm in the simulated transient hole). We do not provide detailed parameters of all site energies used to obtain the fits shown in Figure 4A−D, since, with the exception of the A44/B37 pair (which is discussed in more detail below), these parameter sets were unable to provide reasonable fits to the persistent HB spectrum. The contribution of different Chls to the lowest-energy excitonic state for the four combinations shown in Figure 4 are discussed in the next section.

3.4. Delocalization of the Excited States for Various Combinations of Chls Contributing to the A and B States. To address the issue of the density of the first (i.e., lowest-energy; $\alpha = 1$) exciton state ($d_\alpha(\omega)$, eq 4) and the corresponding Chl distribution ($d_n(\omega)$, eq 5), the calculated absorption spectra (equivalent to those reported in Figure 4, frames A, B, and C) are shown as long-dashed line spectra in the top panels of Figure 5. We recall that these spectra were obtained with the following combinations of Chls corresponding to states A/B: A41/B44 (frame A), A37/B44 (frame B), and A44/B37 (frame C). The shaded narrow bands (top panels) in Figure 5 represent the densities of the lowest-energy exciton state ($\alpha = 1$) of the 13 Chls of the CP43 complex; higher-energy states are not shown for brevity. The middle panels of Figure 5 show the distribution of Chls contributing to state $\alpha = 1$. The corresponding averaged occupation number of the Chls contributing to this state is shown in the lower panels. These data show that the lowest excitonic state is contributed to mainly by two or three pigments. For example, the lowest-energy state in frame A is dominated by Chl 41/Chl 44/Chl 48. In contrast, the lowest-energy state in frames B and C is mostly contributed to by two pigments, that is, Chl 37/Chl 44 (frame B) and Chl 44/Chl 37 (frame C), with relatively smaller contribution from a third pigment (i.e., Chl 45 in frame B and Chl 42 in frame C). As shown in Figure 4A−C, all these A/B combinations provided good fits to both absorption and transient HB spectra and were chosen as possible combinations to simultaneously fit the persistent HB spectrum.

3.5. Comparison of Calculated and Experimental Transient and Persistent Holes Obtained under Non-Line-Narrowing Conditions. As discussed in detail in paper I, we believe that it is not necessary to invoke novel hole-burning mechanisms, such as the photoconversion suggested by Hughes et al., to account for the broad photoproduct distribution observed in the 14 700−15 000 cm^{-1} range of the persistent HB spectrum of CP43 (see solid line in frame B of Figure 6), because simple redistribution of oscillator strength of Chls during the HB process due to modified excitonic interactions could account for the same behavior. To test this idea, simulations of the highly characteristic persistent HB spectrum of CP43 were performed using the combination of A/B pigments discussed above.

Since modeling of nonphotochemical hole burning requires not only identification of the lowest energy trap state in each simulated "complex", but also proper placement of the antihole (i.e., the "post-burn" site energy of the lowest-energy pigment), the process is more complex to directly model. Fortunately, experimental data provide key information on antihole distributions which can be used in simulations. Most importantly, the experimental data reported in the preceding paper I show that the significant fraction of the antihole from the B state is shifted slightly to the red of the 683-nm peak, at least at low-burn fluences. Photoproduct from the A state, on the other hand, is largely shifted blue, as evidenced by the absence of photoproduct to the red of the persistent hole. The antihole placement for the remaining (non-A/B) pigments is more difficult to establish, but since in the calculations presented here the lowest energy state is largely contributed by the A_s and B_s substates, the contribution of these non-A/B pigments to the persistent hole is less critical. Details on photoproduct distributions used in the calculated spectrum are described below and in the Materials and Methods section of the paper.

To determine which A/B pigment combinations could give reasonable fits to the persistent hole spectra, simulations were carried out for each of the site energy combinations corresponding to the spectra shown in Figure 5 (along with many others) using these experimental observations as guidelines. The antihole for A-state pigments was placed within a Gaussian distribution either shifted slightly to the blue or unshifted from the original A-state SDF. It should be emphasized at this point that because the simulation "burns" only those pigments *which are the lowest energy in their complex*, only pigments on the low-energy side of their respective SDF are burned. As a result, even photoproduct placed within the corresponding pigment's "preburn" SDF will result in a net blue shift of the pigment distribution and a corresponding low-energy bleach with antihole toward higher energy. To produce a red-shifted peak such as that observed experimentally for the B-state, the "postburn" SDF had to be shifted to the red by a value between 10 and 30 cm^{-1}, depending on the particular set of site energies used. Various antihole distribution parameters were tested for the non-A/B pigments; however, because of the relatively small contribution of these pigments to the lowest energy state, these parameters had little effect on the broad features of the calculated spectra.

Of the three site energy combinations discussed above (i.e., A41/B44, A37B44, and A44/B37) only the A44/B37 pair showed significant response in the 670-nm region during simulations of the persistent hole-burned spectra. To confirm this result, simulations were repeated with a wide variety of parameters for each of the A/B combinations shown in Figure 5 as well as for a number of others. Both site energies and antihole distribution functions were modified in an attempt to fit the experimental data. Interestingly, only those combinations in which Chl 44 is selected as the A-state pigment showed any response in the 670-nm region. (Other combinations which showed mild response near 670 nm include A44/B34, A44/B49, and A44/B41, although the response was weaker than for the A44/B37 combination). This is in agreement with the results of the transient hole simulations discussed in Section 3.3, and strongly suggests that Chl 44 plays a critical role in formation of the 670-nm antihole observed experimentally.

Figure 6 shows calculated spectra for an optimized set of parameters (see Table 2) for the A44/B37 pair obtained using a fitting algorithm similar to that discussed above together with manual "tweaking" of specific parameters. (In particular, the fitting algorithm tended to broaden the 683 nm band, as shown in frame C of Figure 4, requiring slight adjustments to be made to the site energies and distribution widths of the lowest energy pigments.) The persistent hole spectrum was then fitted using the site energies and SDF widths provided by the fits to the absorption and transient HB spectra accompanied by manual adjustment of postburn SDF parameters (i.e., photoproduct distribution shifts and widths) to match experimental spectra. Frame A of Figure 6 shows the experimental CP43 absorption spectrum (smooth, solid curve) and transient hole spectrum (noisy, gray curve) along with the calculated absorption (long-

dashed curve) and triplet bottleneck holes (smooth black solid and dotted hole spectra). The dotted transient hole-burned curve corresponds to the calculated transient hole-burned spectrum when Chl 44 (pigment A) contributes to the spectrum with twice the efficiency of all other Chls; note the increased hole depth in the 670-nm region. Frame B shows the experimental (solid curve) and calculated (dashed curve) low-fluence persistent hole spectra. In calculations, photoproduct placement was assumed to be uncorrelated with the preburn site energy of the burned pigment. The nonphotochemically burned Chl 44 was placed randomly within the original Chl 44 distribution function. To reproduce the red-shifted antihole observed experimentally, the B state (i.e., Chl 37) antihole distribution is shifted 25 cm^{-1} to the red of the preburn B-state SDF. The postburn SDFs for the remaining (non-A/B) pigments were assigned a width of 70 cm^{-1} and centered at 14 650 cm^{-1}, a blue shift of 25 cm^{-1} from the maximum depth of the transient hole spectrum calculated with no contribution from either A or B pigments (i.e., Chls 37 and 44). It is significant that of the likely A/B candidates tested here, only the A44/B37 combination was capable of simultaneously fitting the transient HB, persistent HB, and absorption spectra (as well as the emission spectrum, as will be discussed below).

3.6. Delocalization of the Excited States for the Best Combination of Chls Contributing to the A and B States. The density of the first (solid line), second (dash−dotted line), and third (dotted curve) exciton states for the set of site energies and SDF widths given in Table 2 is shown in Figure 7 (frame A). The long dashed spectrum corresponds to the calculated absorption spectrum and is shown here for comparison. The averaged oscillator strength of the lowest three exciton states is 0.91, 1.04, and 1.51, respectively, while the averaged occupation number of the first three exciton states is 1.36, 1.65, and 2.36, respectively. The left and right inserts in frame A of Figure 7 show the averaged occupation number of the major Chs contributing to the first and second exciton states ($\alpha = 1$ and $\alpha = 2$, respectively). Note that about 82% of the oscillator strength in the first exciton state originates from two Chls, that is, Chl 37 (47.5%) and Chl 44 (34.4%); Chl 45 (whose contribution to the first exciton state is only ~10%) contributes mostly to the third exciton state (~30%; data not shown). Although Chls 37 and 44 contribute mostly to the first and second exciton states, a small contribution from these pigments, especiallly Chl 44, to higher-energy exciton states is clearly revealed in frame B of Figure 7, where the distribution functions, $d_n(\omega)$, of Chl 37, 44, 45, and 34 are plotted as a function of energy. Other Chls (i.e., Chls 34, 35, 41−43, and 46−49) mostly contribute to the higher-energy exciton states ($\alpha > 2$), predominantly on the blue side of the absorption spectrum. It is interesting to note that for this set of parameters, the two lowest energy exciton states, $\alpha = 1$ and $\alpha = 2$, each have significant contributions from both the lumenal layer (Chl 37) and the stromal layer Chls (Chl 44). We associate the above groups of Chls 34/37 and 44−47 with the states B and A discussed in paper I, with Chls 37 and 44 being the major contributors to the states B and A, respectively. Importantly, the relative contribution from states A and B to the two lowest-energy overlapping exciton states is in good agreement with the analysis of experimental data presented in paper I.

It should be noted here that for simplicity, except for the dotted curves shown in frame C of Figure 4 and frame A of Figure 6, the calculations presented here assume an equal probability for A- and B-type pigments to contribute to HB spectra. This may not, in fact, be the case, since a variety of factors could easily result in greater or lesser contributions of individual pigments to HB spectra (e.g., triplet lifetime and intersystem crossing rates in transient HB spectra and burning efficiencies in persistent HB spectra). In particular, it has been suggested that the A state should contribute primarily to the transient HB spectrum and that the B state should exhibit a much higher hole-burning efficiency at low fluence.[14,15] Such factors were investigated in modeling of both persistent and transient HB spectra by assigning different burning efficiencies to various pigments in the simulations. As shown in frame C of Figure 4 and frame A of Figure 6, it was found that allowing the A state to contribute more strongly (but not exclusively) to the transient HB spectrum does provide somewhat better fits, in good agreement with the analysis of refs 15 and 36. In fact, by varying the contributions of various pigments to the transient HB spectrum, it was found that the bleach near 670 nm is due almost entirely to the excitonic interactions of Chl 44 with higher energy pigments (see Figure 7 frame B). The depth of the bleach can be adjusted in calculations by adjusting the relative contribution of Chl 44 (the A-state) to the calculated transient HB spectrum. In simulations where the contribution of Chl 44 was neglected entirely, no bleach was observed in the 670 nm region (data not shown). Likewise, by varying burning efficiencies in persistent HB simulations, it was found that the 670 nm antihole is due almost entirely to redistribution of oscillator strength, which occurs during NPHB of Chl 44. (In simulations where Chl 44 was assigned a burning efficiency of 0, no antihole was observed in the 670-nm region.) This is in agreement with our earlier noted finding (see Sections 3.3 and 3.5) that only those A/B combinations in which Chl 44 was either the A or B pigment provided reasonable fits to the transient and persistent HB spectra. Interestingly, assigning a higher burning efficiency to the B state in persistent HB simulations did not meaningfully improve the fit, since minor adjustments to antihole distribution parameters could produce the same effect. In fact, good fits could be obtained to the experimental persistent HB spectrum, assuming a wide variety of burning efficiencies (with either A or B assigned a higher burning efficiency) so long as Chl 44 was chosen as the A state. More detailed experimental information on antihole distributions will be required to accurately assess burning efficiencies.

In summary, our calculations strongly suggest that both the transient and persistent HB spectra have significant contribution from an A state localized primarily on Chl 44. These calculations are in excellent agreement with our model of uncorrelated excitation energy transfer between quasidegenerated states A and B, as presented in paper I and in ref 36, where we argued that Chls in lumenal and stromal layers are connected by efficient EET. In addition, since persistent holes can be fitted (see Figure 6) without invoking a special photoconversion mechanism as suggested by Hughes et al.[15] (vide supra), our results strongly support the idea that the very broad and positive absorbance increase observed in the persistent nonphotochemical holes originates from the redistribution of oscillator strength due to modified excitonic interactions, rather than the unique photoconversion mechanism involving Chl−protein H-bonding proposed in ref 15.

3.7. Comparison of Calculated and Experimental Fluorescence Spectrum. The calculated emission spectrum of CP43 is compared with the experimental spectrum shown in Figure 8. The dashed curve (c) represents the experimental spectrum obtained for our best CP43 sample (i.e., our sample with the largest B state absorption at 683 nm and the smallest contribution from aggregated complexes which have an absorption

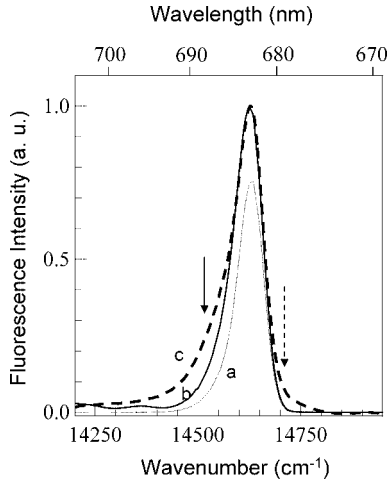

Figure 8. Spectrum a is the calculated site distribution function of the $\alpha = 1$ lowest energy state, with main contributions from Chl 37 and Chl 44. Spectrum b is this site distribution function dressed with phonons and chlorophyll molecular vibrations. The dashed curve, c, represents the experimental fluorescence spectrum obtained for our best CP43 sample. The solid and dashed arrows point to other contributions as discussed in text.

maximum near 685−687 nm; see paper I). Curve a is the calculated SDF of the lowest energy state ($\alpha = 1$) from Figure 7A. The relative contributions of Chl 37 and Chl 44 to this curve are the same as in the triplet-bottleneck hole-burned spectra in Figure 6A. Spectrum b is this site distribution function dressed with phonons and chlorophyll molecular vibrations (convoluted with single molecule emission spectrum), that is, the theoretical emission spectrum. Both spectra exhibit the same asymmetric shape and are peaked within 2−3 cm^{-1} of each other (taking into account the resolution of the spectrograph and the precision of theoretical SDF calculation, this discrepancy is negligible). The two vertical arrows indicate the regions of the largest discrepancies between theoretical and experimental spectra. The solid arrow at 688 nm corresponds to the region where emission from aggregated CP43 complexes is expected (see paper I and ref 14). Because our calculations obviously did not take such aggregation (or any other intercomplex interactions) into account, a discrepancy in this region is expected. Similarly, as discussed in paper I, emission at 679 nm (dashed arrow) can be ascribed either to a small amount of contaminant (observed in some CP43 preparations as discussed in paper I; see Figure 2B) or from a small subpopulation of CP43 complexes in which some emission originates from $\alpha > 1$ states. That is, for a small number of specific realizations of the energy disorder, emission near 678 - 679 nm could be observed if the EET from the higher-energy excitonic states ($\alpha > 1$) to the lowest-energy state ($\alpha = 1$) is inefficient.

3.8. On the Nature of Chls Contributing to the Lowest-Energy Band near 683 nm. The availability of relatively high-resolution X-ray structural data has made it possible (at least in principle) to link spectroscopic data on individual excitonic states with the structural data regarding the local environment of individual pigments. For example, Di Donato et al.[8] have recently presented an analysis of femtosecond visible/visible and visible/mid-infrared pump/probe spectroscopic data on the CP43 low-energy states in terms of hydrogen bonding and ligation status of individual pigments to the protein environment. Although several low-energy candidates were considered (i.e., Chls 34, 37, 41, 47, and 49), no specific assignments were proposed. While we do not wish to put too much emphasis on an interpretation of protein−ligand interactions based on the current structure, some observations are in order. We hasten to add that specific assignments of hydrogen bonding or ligand interactions are, at the current resolution, speculative since (1) water molecules (which the higher resolution structure of PSI demonstrates can very frequently act as H-bond donors) are not resolved and (2) at 3.0-Å resolution, the orientation of specific protein side chains is necessarily somewhat imprecise, leaving significant room for error.

Frames A−D of Figure 9 show the four Chl molecules that, as discussed above, we consider as the most likely candidates contributing to states A and B. To briefly address the possibility of H-bonding and ligand coordination, the relevant nearby residues and cofactors are also shown. Frame A shows that Chl 34 is very close to the His 430 ligand and reveals a potential H-bonding to Tyr 297c, although bonding is probably stronger to both the short-chain ester carbonyl of Chl 34 and the long-chain ester carbonyl of Chl 33. Frame B shows the environment of Chl 37 which, interestingly, does not appear to be coordinated by a His residue, as are most of the other Chl in the CP43 complex. Instead, the most obvious ligand for Chl 37 seems to be the carbonyl O of Dgd 205, which has an ester carbonyl group oriented well for ligation and only 3.2 Å from the central Mg atom of Chl 37. We have tentatively assigned Chl 37 to be β-ligated, although it is possible that the Met 67 residue (which has a sulfur atom 4.3 Å away from Chl 37's center Mg atom) could instead act as an α-ligand, either directly or through binding water molecules (which are not resolved in this structure), as suggested by Di Donato et al.[8] Ligation through water molecules has been observed in several binding sites in PSI (e.g., His 240A with Chl A14, and Glu 98F and Ile 717A with Chl A39; see the 2.5-Å resolution structure of Jordan et al.[39] available under PDB ID 1JB0). We recall that Chl 37 was identified as the pigment mostly contributing to state B, which (as shown above and in paper I) is characterized by a relatively narrow inhomogeneous broadening. Interestingly, the current crystal structure places the terminal C atom of the Met 67 residue within 2.6 Å of the Chl 37 Mg atom, which seems physically unlikely. Final assignment of the ligation status must await a better resolution crystal structure or use of high resolution spectroscopic data. Frame C shows Chl 41 and a possible H-bond donor for the 13′ carbonyl group (Tyr 274c), as suggested by Hughes et al.[15] The Tyr 274c phenolic OH group is within 4 Å of the 13′ carbonyl of Chl 41, although it appears that the phenolic OH of Tyr 274c may be better positioned for H-bonding with the nearby OH group of Ile 265 than with the 13′ carbonyl of Chl 41. In addition, although H-bonding for this particular Chl is quite feasible, the modeling studies presented above suggest that this Chl does not constitute a low-energy trap, in contrast to the suggestion of Hughes et al.[15] and predictions by Vasil'ev et al.[13] and Saito et al.,[34] where it was suggested that Chl 41 plays the most important role in transferring energy to the RC of PSII. Finally, Chl 44, together with important nearby residues, is shown in frame D of Figure 9. Here, several polar residues (i.e., His 444, Glu 269, and Arg 447c), along with a phospholipid (Lhg 203, not shown), are close by that could lead to the red-shift of this pigment (in agreement with our QM calculations, vide supra) and our modeling studies. (Interestingly, charged residues Arg 447c and Glu 269c appear to form a salt bridge nearby.) Although no obvious H-bonds between the 13′ carbonyl of Chl 44 and the surrounding protein are observed, the polarity of its local environment makes it very possible that such interactions might be found in future, higher-resolution structures. Chl 44 is clearly ligated by His 444, although since there are no close lying

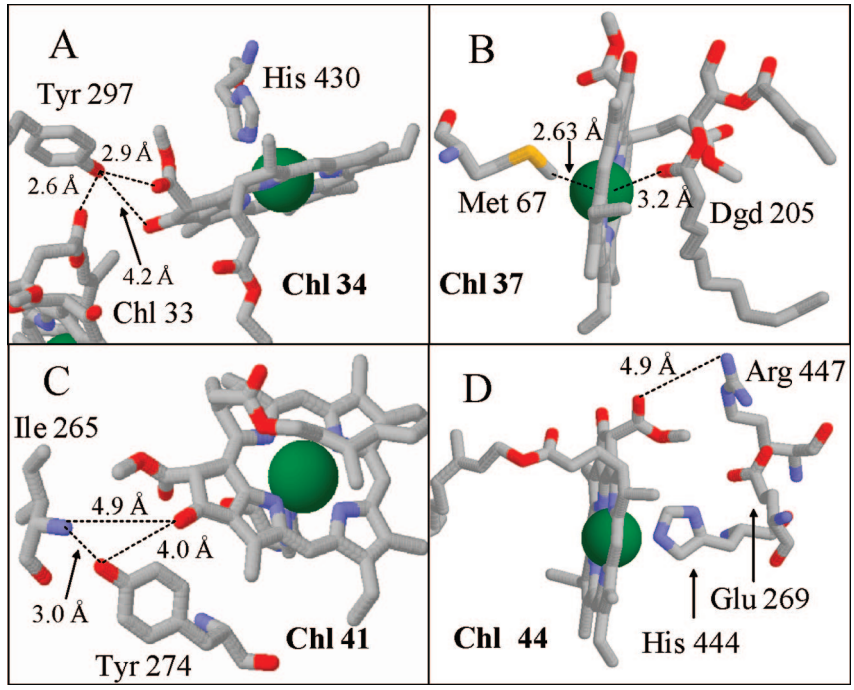

Figure 9. CP43 chlorophylls[6] of interest as low-energy state candidates, together with relevant nearby residues and cofactors. Frame A: Chl 34 with ligand His 430, Chl 33, and potential H-bond donor Tyr 297. Frame B: Chl 37 along with Met 67 and Dgd 205, possible ligands. Frame C: Chl 41 with potential H-bond donor Tyr 274 and nearby Ile 265 (ligand His 441 is hidden beneath the Chl). Frame D: Chl 44 shown with ligand His 444 and nearby charged residues Arg 447 and Glu 269, which appear to be involved in a salt bridge.

residues in the vicinity of the central Mg on the opposite side, a second ligation by a water molecule cannot be excluded. On the basis of the above discussion, it is clear that the coordination status of the Chls assigned to the low-energy traps remains an open question and requires further studies. This question is currently under investigation in our laboratory using high-resolution FLNS studies by comparing selectively excited CP43 FLN spectra with spectra obtained for isolated Chls in penta- and hexa-coordinating solvents under identical conditions.

4. Conclusions

A set of site energies for the CP43 chlorophylls is provided that can simultaneously describe several types of optical spectra. The excitonic structure was probed by Monte Carlo simulations using a simple fitting algorithm that provided very good fits to absorption, emission, persistent, and transient HB spectra. The shape of the calculated lowest-energy state, its composition, and exciton state Chl distribution function are consistent with experimental data and our model for excitation energy transfer between two quasi-degenerate lowest-energy states (A and B) with uncorrelated SDFs (see paper I). That is, the 4.2 K asymmetric triplet-bottleneck (transient) hole was shown to be mostly contributed to by both A and B states, with the hole profile described by a subensemble of pigments, which are the lowest-energy pigments in their complexes. The same lowest-energy Chls contribute to the observed fluorescence spectra. In addition, our excitonic calculations showed that absorption changes observed near 670 nm in the nonline narrowed persistent HB spectra (assigned previously to photoconversion that involves Chl−protein hydrogen bonding[15]) are most likely the result of NPHB accompanied by the redistribution of oscillator strength due to modified excitonic interactions. Moreover, it has been shown that a unique redistribution of oscillator strength during the NPHB process necessary to fit the persistent HB spectrum helped to assign Chls contributing to the low-energy states; namely, Chl 44 for state A and Chl 37 for state B. Although our results presented in this paper are consistent with the B1A1 model discussed in paper I, in which band A is due to a state well-localized on Chl 44, the model of Hughes et al.,[15] that is, BMA1, where M stands for multiple pigments contributing to the B band, cannot be excluded until low-temperature LD and CD spectra (obtained for monomeric CP43 complexes, i.e. free of aggregates) become available for simultaneous fits with optical spectra discussed in this manuscript. In summary, our results provided more insight into the nature of the low-energy trap in the CP43 complex, which plays an important role in light-harvesting and photoprotection of PSII. More advanced excitonic theories will be applied to the system studied in this work when a direct calculation of site energies from structural data is available from more advanced QM theory and a higher resolution crystal structure.

Abbreviations

Chlorophyll, Chl; coupling constants, V_{nm}; delocalization, N_{del}; density of exciton states, $d_\alpha(\omega)$; energy, E; excitation energy transfer, EET; exciton states Chl distribution, $d_n(\omega)$; fluorescence line-narrowing, FLN; full width at half-maximum, fwhm; Huang−Rhys factor, S; inhomogeneous broadening, Γ_{inh}; kiloDalton, kD; nonphotochemical hole burning, NPHB; pheophytin, Pheo; photochemical hole burning, PHB; phonon sideband, PSB; photosystem I, PSI; photosystem II, PSII; reaction center, RC; site distribution function, SDF; spectral hole-burning, SHB; temperature, T; zero-phonon line, ZPL.

Acknowledgment. This work was supported by the start-up funding at the Department of Chemistry, Kansas State University (R.J.) and in part by the U.S. Department of Energy (US-DOE), EPSCoR grant (R.J.) and Energy Biosciences Program, Basic Energy Sciences, US-DOE (M.S.). V.Z. acknowledges support by NSERC.

References and Notes

(1) Blankenship, R. E. In *Molecular mechanisms of photosynthesis*; Blackwell Science: Oxford; Malden, MA: 2002; Chapters 4−6, pp 42−123.

(2) Barber, J.; Anderson, J. M. Introduction to "Photosystem II: Molecular Structure and Function, Meeting Held at the Royal Society 13−14 March 2002;. *Philos. Trans. R. Soc. London, B (* **2002)** , *357*, 1325–1328.

(3) Archer, M. D.; Barber, J. Molecular to Global Photosynthesis. *Ser. Photoconvers. Sol. Energy* **2004**, 1–42, Chapter 1.

(4) Barber, J. Photosystem II: The Engine of Life. *Q. Rev. Biophys.* **2003**, *36*, 71–89.

(5) Diner, B. A.; Rappaport, F. Structure, Dynamics, and Energetics of the Primary Photochemistry of Photosystem II of Oxygenic Photosynthesis. *Annu. Rev. Plant Biol.* **2002**, *53*, 551–580.

(6) Loll, B.; Kern, J.; Saenger, W.; Zouni, A.; Biesiadka, J. Towards Complete Cofactor Arrangement in the 3.0 Å Resolution Structure of Photosystem II. *Nature* **2005**, *438*, 1040–1044.

(7) Bricker, T. M.; Frankel, L. K. The Structure and Function of CP47 and CP43 in Photosystem II. *Photosynth. Res.* **2002**, *72*, 131–146.

(8) Di Donato, M.; van Grondelle, R.; van Stokkum, I. H.; Groot, M. L. Excitation Energy Transfer in the Photosystem II Core Antenna Complex CP43 Studied by Femtosecond Visible/Visible and Visible/Mid-Infrared Pump Probe Spectroscopy. *J. Phys. Chem. B* **2007**, *111*, 7345–7352.

(9) De Weerd, F. L.; Van Stokkum, I. H. M.; Van Amerongen, H.; Dekker, J. P.; Van Grondelle, R. Pathways for Energy Transfer in the Core Light-Harvesting Complexes CP43 and CP47 of Photosystem II. *Biophys. J.* **2002**, *82*, 1586–1597.

(10) Vasil'ev, S.; Orth, P.; Zouni, A.; Owens, T. G.; Bruce, D. Excited-State Dynamics in Photosystem II: Insights from the X-ray Crystal Structure. *Proc. Natl. Acad. Sci. U.S.A.* **2001**, *98*, 8602–8607.

(11) Raszewski, G.; Saenger, W.; Renger, T. Theory of Optical Spectra of Photosystem II Reaction Centers: Location of the Triplet State and the Identity of the Primary Electron Donor. *Biophys. J.* **2005**, *88*, 986–998.

(12) Jankowiak, R.; Hayes, J. M.; Small, G. J. An Excitonic Pentamer Model for the Core Q_y States of the Isolated Photosystem II Reaction Center. *J. Phys. Chem. B* **2002**, *106*, 8803–8814.

(13) Vasil'ev, S.; Bruce, D. A Protein Dynamics Study of Photosystem II: The Effects of Protein Conformation on Reaction Center Function. *Biophys. J.* **2006**, *90*, 3062–3073.

(14) Jankowiak, R.; Zazubovich, V.; Rätsep, M.; Matsuzaki, S.; Alfonso, M.; Picorel, R.; Seibert, M.; Small, G. J. The CP43 Core Antenna Complex of Photosystem II Possesses Two Quasi-Degenerate and Weakly Coupled Q_y-Trap States. *J. Phys. Chem. B* **2000**, *104*, 11805–11815.

(15) Hughes, J. L.; Picorel, R.; Seibert, M.; Krausz, E. Photophysical Behavior and Assignment of the Low-Energy Chlorophyll States in the CP43 Proximal Antenna Protein of Higher Plant Photosystem II. *Biochemistry* **2006**, *45*, 12345–12357.

(16) Hughes, J. L.; Prince, B. J.; Krausz, E.; Smith, P. J.; Pace, R. J.; Riesen, H. Highly Efficient Spectral Hole-Burning in Oxygen-Evolving Photosystem II Preparations. *J. Phys. Chem. B* **2004**, *108*, 10428–10439.

(17) Groot, M.; Frese, R. N.; De Weerd, F. L.; Bromek, K.; Pettersson, A.; Peterman, E. J. G.; Van Stokkum, I. H. M.; Van Grondelle, R.; Dekker, J. P. Spectroscopic Properties of the CP43 Core Antenna Protein of Photosystem II. *Biophys. J.* **1999**, *77*, 3328–3340.

(18) Zouni, A.; Witt, H. T.; Kern, J.; Fromme, P.; Krauss, N.; Saenger, W.; Orth, P. Crystal Structure of Photosystem II from Synechococcus Elongatus at 3.8 Å Resolution. *Nature* **2001**, *409*, 739–743.

(19) Krawczyk, S. Hydrogen Bonding and Desolvation of Chlorophyll A in Mixed Basic and Protic Solvents. *Annales Universitatis Maria Curie-Sklodowska, Section AAA: Physica* **1993**, *48*, 101–109.

(20) Krawczyk, S. The Effects of Hydrogen Bonding and Coordination Interaction in Visible Absorption and Vibrational Spectra of Chlorophyll a. *Biochim. Biophys. Acta* **1989**, *976*, 140–149.

(21) Balaban, T. S. Are Syn-Ligated (Bacterio)Chlorophyll Dimers Energetic Traps in Light-Harvesting Systems. *FEBS Lett.* **2003**, *545*, 97–102.

(22) Balaban, T. S.; Fromme, P.; Holzwarth, A. R.; Krauss, N.; Prokhorenko, V. I. Relevance of the Diastereotopic Ligation of Magnesium Atoms of Chlorophylls in Photosystem I. *Biochim. Biophys. Acta* **2002**, *1556*, 197–207.

(23) Gudowska-Nowak, E.; Newton, M. D.; Fajer, J. Conformational and Environmental Effects on Bacteriochlorophyll Optical Spectra: Correlations of Calculated Spectra with Structural Results. *J. Phys. Chem.* **1990**, *94*, 5795–5801.

(24) Zucchelli, G.; Brogioli, D.; Casazza, A. P.; Garlaschi, F. M.; Jennings, R. C. Chlorophyll Ring Deformation Modulates Q_y Electronic Energy in Chlorophyll-Protein Complexes and Generates Spectral Forms. *Biophys. J.* **2007**, *93*, 2240–2254.

(25) Knox, R. S.; Spring, B. Q. Dipole Strengths in the Chlorophylls. *Photochem. Photobiol.* **2003**, *77*, 497–501.

(26) Singh, I. S.; Becker, R. S. π-π* Phosphorescence of Chlorophylls *a* and *b*. *J. Am. Chem. Soc.* **1960**, *82*, 2083–2084.

(27) Jankowiak, R.; Tang, D.; Small, G. J.; Seibert, M. Transient and Persistent Hole Burning of the Reaction Center of Photosystem II. *J. Phys. Chem.* **1989**, *93*, 1649–1654.

(28) Tang, D.; Jankowiak, R.; Seibert, M.; Small, G. J. Effects of Detergent on the Excited State Structure and Relaxation Dynamics of the Photosystem II Reaction Center: A High-Resolution Hole Burning Study. *Photosynth. Res.* **1991**, *27*, 19–29.

(29) Chang, H.-C.; Jankowiak, R.; Reddy, N. R. S.; Small, G. J. Pressure Dependence of Primary Charge Separation in a Photosynthetic Reaction Center. *Chem. Phys.* **1995**, *197*, 307–321.

(30) Jentzen, W.; Song, X.; Shelnutt, J. A. Structural Characterization of Synthetic and Protein-Bound Porphyrins in Terms of the Lowest-Frequency Normal Coordinates of the Macrocycle. *J. Phys. Chem. B* **1997**, *101*, 1684–1699.

(31) Liu, Z.; Yan, H.; Wang, K.; Kuang, T.; Zhang, J.; Gui, L.; An, X.; Chang, W. Crystal Structure of Spinach Major Light-Harvesting Complex at 2.72 Å Resolution. *Nature (London)* **2004**, *428*, 287–292.

(32) Ferreira, K. N.; Iverson, T. M.; Maghlaoui, K.; Barber, J.; Iwata, S. Architecture of the Photosynthetic Oxygen-Evolving Center. *Science* **2004**, *303*, 1831–1838.

(33) Riley, K. J.; Zazubovich, V.; Jankowiak, R. Frequency-Domain Spectroscopic Study of the PS I-CP43′ Supercomplex from the Cyanobacterium Synechocystis PCC 6803 Grown Under Iron Stress Conditions. *J. Phys. Chem. B* **2006**, *110*, 22436–22446.

(34) Saito, K.; Kikuchi, T.; Nakayama, M.; Mukai, K.; Sumi, H. A Single Chlorophyll in each of the Core Antennas CP43 and CP47 Transferring Excitation Energies to the Reaction Center in Photosystem II of Photosynthesis. *J. Photochem. and Photobiol., A* **2006**, *178*, 271–280.

(35) Hughes, J. L.; Prince, B. J.; Arskold, S. P.; Krausz, E.; Pace, R. J.; Picorel, R.; Seibert, M. Photo-Conversion of Chlorophylls in Higher-Plant CP43 Characterized by Persistent Spectral Hole Burning at 1.7 K. *J. Lumin.* **2004**, *108*, 131–136.

(36) Zazubovich, V.; Jankowiak, R. On the Energy Transfer between Quasi-Degenerate States with Uncorrelated Site Distribution Functions: An Application to the CP43 Complex of Photosystem II. *J. Lumin.* **2007**, *127*, 245–250.

(37) Damjanovic, A.; Vaswani, H. M.; Fromme, P.; Fleming, G. R. Chlorophyll Excitations in Photosystem I of Synechococcus Elongatus. *J. Phys. Chem. B* **2002**, *106*, 10251–10262.

(38) Manna, P.; Vermaas, W. Mutational Studies on Conserved Histidine Residues in the Chlorophyll-Binding Protein CP43 of Photosystem II. *Eur. J. Biochem.* **1997**, *247*, 666–672.

(39) Jordan, P.; Fromme, P.; Witt, H. T.; Klukas, O.; Seanger, W.; Krauss, N. Three-Dimensional Structure of Cyanobacterial Photosystem I at 2.5Å Resolution . *Nature (London)* **2001**, *411*, 909−917.

(40) Dang, N. C.; Zazubovich, V.; Reppert, M.; Neupane, B.; Picorel, R.; Seibert, M.; Jankowiak, R. *J. Phys. Chem. B* **2008**, *112*, 9921–9933.

JP8013749